dependence of the minimum turning radius on $(L/D)_{max}$ in Eq. (17b), although the minimum radius turn does not occur at $(L/D)_{max}$ because α_* also depends on τ, as can be seen from Eq. (17a). The inequality of Eq. (10) now becomes

$$\frac{1}{\tau}\left(\frac{1-\tau^2}{C_{D_0}}\right)^{1/3} \leq n_{lim} \tag{18}$$

It is also noteworthy (see Fig. 2) that the tightest turn does not necessarily occur at the limiting load factor, as is the case at low speeds if τ is high enough.[2] Using Eqs. (15) and (17a), the approximate expressions for the flight conditions become

$$\frac{V_*}{V_s} \approx \left[\frac{3(1-\tau^2)}{3-\tau^2}\right]^{1/2} \tag{19}$$

$$\rho_* \approx \frac{2\tau}{3C_{D_0}R_0}\left(\frac{m}{A}\right) \tag{20}$$

The velocity is predicted very well by Eq. (19), while Eq. (20) overpredicts the altitudes by up to 4% (see Fig. 3).

Lastly, the validity of assuming a constant vehicle weight during the turn is examined. Consider the case of a 60 deg turn, or heading change, at a constant 1000-km radius for $\tau = 0.88$. The optimum speed is 4.42 km/s, from Fig. 3, which gives a time of 237 s, or nearly 4 min. Assuming an efficient, air-breathing propulsion system with a specific impulse of 2000 s gives a fuel consumption equal to 10% of the vehicle's weight at the inception of a 60 deg turn. While the vehicle's weight change during a turn is not negligible, the assumption of constant weight made here can be justified on the basis that the present, simplified analysis provides physical insight that is absent in numerical calculations.

Conclusions

An analytic formulation for the case of coordinated, constant altitude and speed, minimum-radius, hypervelocity turns is presented. Some example calculations, performed using approximate aerodynamics based on Newtonian theory, lead to the following conclusions: 1) at hypervelocity speeds, turning radii are very large, typically 500–1500 km; 2) the optimum, constant flight velocities are high, ranging from 3 to 5 km/s; 3) the maneuver must be performed at high altitudes, near 45 km for a wing loading of 300 kg/m^2; 4) large in-flight values of thrust-to-weight ratio are required, in the vicinity of 0.8 to 0.9; 5) the minimum turning radius is inversely proportional to the vehicle's maximum L/D, although the maneuver is not performed at maximum L/D; and 6) in contrast to low-speed turns, the tightest hypervelocity turns are not necessarily performed at the limiting load factor.

Acknowledgment

The author thanks his colleague, D. B. Kirk, for reviewing the paper and making valuable comments.

References

[1]Vinh, N. X., Busemann, A., and Culp, R. D., *Hypersonic and Planetary Entry Flight Mechanics,* University of Michigan, Ann Arbor, MI, 1980.

[2]Dommasch, D. O., Sherby, S. S., and Connolly, T. F., *Airplane Aerodynamics*, 2nd ed., Pitman, New York, 1957.

[3]Tauber, M. E., "Hypersonic Maximum Lift/Drag Ratio of Flat Plates with Bluntness and Skin Friction," NASA TM-88338, July 1986.

[4]"Glider Performance Characteristics Report," Boeing Co., New York, Document D2-8080-1, 1963.

Comparison of High-Angle-of-Attack Slender-Body Theory and Exact Solutions for Potential Flow Over an Ellipsoid

Michael J. Hemsch*
Lockheed Engineering and Sciences Co., Hampton, Virginia 23666

Nomenclature

a = half-length of ellipsoid
b = half-span of ellipsoid
C_{NL} = longitudinal distribution of the normal-force coefficient
C_{YL} = longitudinal distribution of the side-force coefficient
C_p = pressure coefficient
c = half-height of ellipsoid
L = body length
M_∞ = Mach number
r_0 = radius of transformed cross section in the circle plane
$S(x)$ = axial distribution of cross-sectional area
W = complex velocity potential, $\phi + i\psi$
u, v, w = Cartesian velocity components in body-axis coordinates (see Fig. 1)
α = angle of attack
β = angle of sideslip
ϵ_{max} = maximum percent error in C_{NL}
θ = angle between crossflow velocity vector and z axis
ν = complex position in transform (circle) plane
σ = complex position in physical plane
ϕ = velocity potential
ψ = stream function

Subscripts

$2D,\alpha$ = two-dimensional solution for crossflow (doublet)
$2D,t$ = two-dimensional solution for thickness (source)
$2D,B$ = two-dimensional solution for thickness (source) for circular body with cross-sectional area $S(x)$
axi = axisymmetric solution for equivalent body
long = longitudinal flow

Introduction

IT is generally assumed that the subsonic/transonic/supersonic slender-body theory of Munk,[1] Jones,[2] Ward,[3] and Spreiter[4] applies only to flows about airframes at small angles of attack. However, Barnwell[5] has recently shown that the theory holds for high angles of attack as well, provided that Sychev[6] scaling is used for the flow variables and $M_\infty \sin\alpha \ll 1$. The purpose of this Note is to demonstrate the accuracy of high-angle-of-attack slender-body theory (HASBT) for bodies with elliptical cross sections by comparison with exact solutions for incompressible, potential flow over an ellipsoid.

High-Angle-of-Attack Slender-Body Theory

Heaslet and Spreiter[7] have presented a three-dimensional composite solution for classic slender-body theory (see also

Received Oct. 21, 1989; revision received Dec. 8, 1989.

*Engineer, staff. Associate Fellow AIAA.

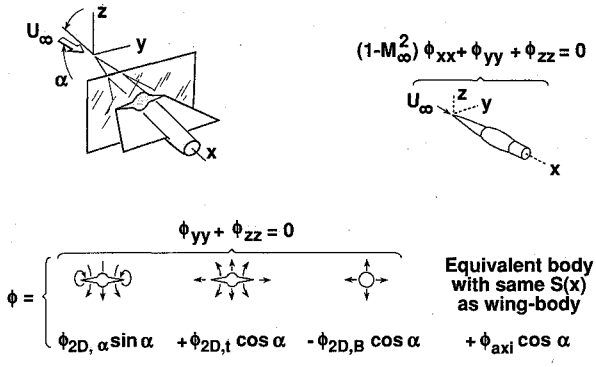

Fig. 1 Decomposition of full-potential equation for $M_\infty \sin\alpha \ll 1$.

the derivation by Ashley and Landahl[8]). A similar HASBT composite solution can be obtained heuristically for an incompressible, potential flow about an arbitrary slender body as follows. The flow is governed by the Laplace equation and can be split into two problems: 1) a purely longitudinal flow with freestream velocity of $U_\infty \cos\alpha$ and 2) a pure crossflow with freestream velocity of $U_\infty \sin\alpha$. The classic slender-body-theory matched asymptotic decomposition[7,8] can be applied to the longitudinal problem with the result

$$\phi_{\text{long}} = (\phi_{2D,t} - \phi_{2D,B} + \phi_{\text{axi}}) \cos\alpha \tag{1}$$

where U_∞ is taken to be 1 and $\phi = 0$ at infinity. The first term of Eq. (1) is the solution for the inner region and satisfies the body-boundary condition. It is obtained by solving the two-dimensional Laplace equation for a growing cross-sectional shape. Hence, the theory of complex variables and conformal mapping may be employed. The third term is the solution for the outer region and is necessary for satisfaction of the boundary condition at infinity.[8] It is obtained by solving the two-dimensional Laplace equation for axisymmetric flow over the "equivalent body," which consists of a body of revolution with the same cross-sectional area distribution. The second term corresponds to two-dimensional flow over cross sections of the equivalent body, and it is necessary for proper combining of the inner and outer solutions.[8] Solutions for ϕ_{axi} can be obtained from line singularity methods.[9]

The solutions for all three terms of Eq. (1) are given by appropriate distributions of source singularities. For the pure crossflow problem, the inner (two-dimensional) solution for each crossflow plane is given by a distribution of doublets and can be obtained by conformal mapping. Since the inner doublet solution satisfies the boundary condition at infinity, no outer solution is needed.[2] Adding the crossflow inner solution to Eq. (1) gives the full HASBT decomposition

$$\phi = \phi_{2D,\alpha} \sin\alpha + (\phi_{2D,t} - \phi_{2D,B} + \phi_{\text{axi}}) \cos\alpha \tag{2}$$

A schematic of the decomposition, following Refs. 5 and 7, is given in Fig. 1.

Two-Dimensional Thickness Problem

The complex potential for the two-dimensional thickness/source terms [second and third terms in Eq. (2)] is given by

$$W[\nu(\sigma)]_{2D,t-2D,B} = \frac{1}{2\pi} S'(x)\{\ln[\nu(\sigma)] - \ln(\sigma)\} \cos\alpha \tag{3}$$

where σ and ν are the complex variables for the physical and transformed (circle) cross-sectional planes, respectively. $S'(x)$ is the derivative with respect to x of the cross-sectional area distribution. Note that ν depends on the cross-sectional geometry as well as on σ.

The velocity components induced by the two-dimensional thickness solution are given by differentiation of Eq. (3). The crossflow plane components are given by differentiation with respect to σ

$$(v - iw)_{2D,t-2D,B} = \frac{1}{2\pi} S'(x) \cos\alpha \left[\frac{1}{\nu}\frac{d\nu}{d\sigma} - \frac{1}{\sigma}\right] \tag{4}$$

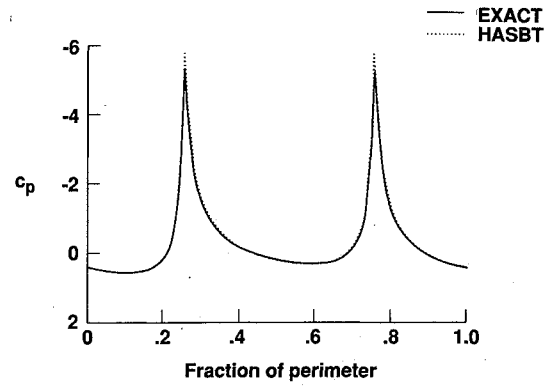

a) Surface pressure distribution at $x/L = 0.25$

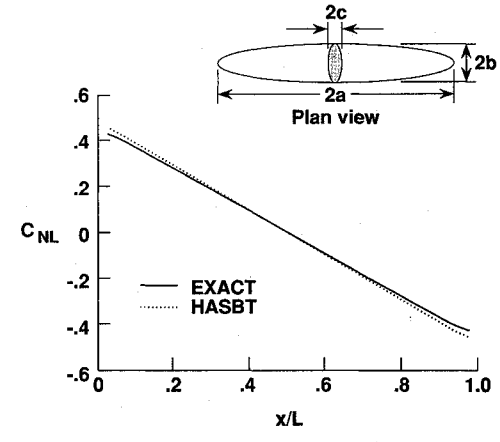

b) Longitudinal distribution of normal-force coefficient

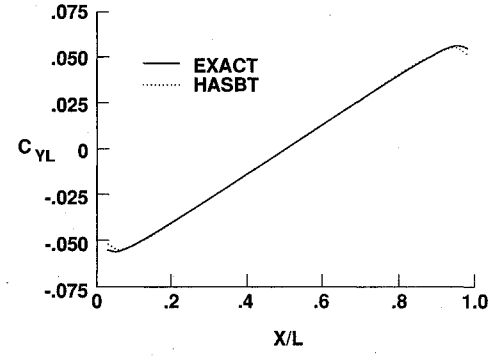

c) Longitudinal distribution of side-force coefficient

Fig. 2 Comparison of exact and HASBT solutions for pressure and force for an ellipsoid with $a/b = 6$, $b/c = 3$, $\alpha = 40$ deg, and $\beta = 15$ deg.

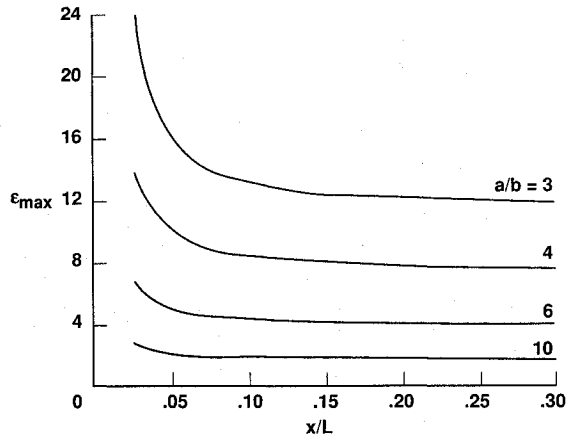

Fig. 3 Maximum percent error in longitudinal normal-force distribution for HASBT solutions for ellipsoids with $1 \le b/c \le 10$.

and the axial component is given by differentiation with respect to x

$$u_{2D,I-2D,B} = Re\left\{\frac{\partial}{\partial x} W[\nu(\sigma)]\right\} \cos\alpha$$

$$= \frac{1}{2\pi} Re\left\{S''(x)[\ell_n(\nu) - \ell_n(\sigma)] + S'(x)\frac{1}{\nu}\frac{\partial \nu}{\partial x}\right\} \cos\alpha \qquad (5)$$

Two-Dimensional Crossflow Problem

The complex potential corresponding to the first term of Eq. (2) is given by

$$W[\nu(\sigma)]_{2D,\alpha} = -ie^{-i\theta}\left(\nu - \frac{r_0^2 e^{2i\theta}}{\nu}\right) \sin\alpha \qquad (6)$$

where r_0 is the radius of the transformed cross section in the circle plane and θ gives the orientation of the crossflow velocity vector. Continuing the procedure carried out in the previous subsection, we find that the crossflow plane velocity components corresponding to Eq. (6) are given by

$$(v - iw)_{2D,\alpha} = -ie^{-i\theta}\left(1 + \frac{r_0^2 e^{2i\theta}}{\nu^2}\right)\frac{d\nu}{d\sigma} \sin\alpha \qquad (7)$$

and the axial component is given by

$$u_{2D,\alpha} = Re\left\{-ie^{-i\theta}\left[\left(1 + \frac{r_0^2 e^{2i\theta}}{\nu^2}\right)\frac{\partial \nu}{\partial x} - \frac{2r_0 e^{2i\theta}}{\nu}\frac{dr_0}{dx}\right]\right\} \sin\alpha \qquad (8)$$

Comparison of HASBT and Exact Solutions

Exact solutions for the incompressible potential flow over an ellipsoid are given by Band and Payne.[10] For comparison with those solutions, Eqs. (4), (5), (7), and (8) must be made specific for elliptical cross sections. The conformal transformation that converts an ellipse into a circle is given by

$$\nu = (1/2)[\sigma + (\sigma^2 - b^2 + c^2)^{1/2}] \qquad (9)$$

with

$$r_0 = (1/2)(b + c) \qquad (10)$$

Carrying out the required differentiations gives

$$\frac{d\nu}{d\sigma} = \frac{\nu}{2\nu - \sigma} \qquad (11)$$

and

$$\frac{\partial \nu}{\partial x} = \frac{(1/2)[-b\ db/dx + c\ dc/dx]}{2\nu - \sigma} \qquad (12)$$

The equivalent body for an ellipsoid is a prolate spheroid whose cross-sectional radius is given by

$$R(x) = \sqrt{(1/\pi)S(x)} \qquad (13)$$

The potential for a prolate spheroid at zero angle of attack and sideslip is given by Wang.[11]

Comparisons of HASBT and exact solutions have been made for a wide variety of ellipsoid geometries and angles of attack and sideslip. A typical result is given in Fig. 2. The length-to-width ratio of the ellipsoid is 6. The width-to-height ratio is 3. The angles of attack and sideslip are 40 and 15 deg, respectively. The full Bernoulli equation was used to compute the pressures from the velocity components.

The excellent accuracy of the pressure distribution for $x/L = 0.25$ is typical except for axial stations close to the blunt tips where the axial gradients are large in violation of the assumptions of slender-body theory. Surprisingly, the level of accuracy appears to be essentially independent of the angles of attack and sideslip. The dependence on fineness ratio of the accuracy of the longitudinal normal-force distribution near the tips is given in Fig. 3 for $1 \le b/c \le 10$. The accuracy is only weakly dependent on b/c. The error curves given in Fig. 3 are for the worst cases. Results for the pressure distributions are comparable.

In conclusion, the addition of the appropriate trigonometric coefficients to the classical slender-body theory decomposition gives the formally correct HASBT and results in accuracies previously thought to be unattainable.

Acknowledgment

This work was supported by the Transonic Aerodynamics Branch of NASA Langley Research Center under Contract NAS1-18000. Helpful discussions with R. M. Hall, J. M. Luckring, and R. W. Barnwell are gratefully acknowledged.

References

[1]Munk, M. M., "The Aerodynamic Forces on Airship Hulls," NACA Rept. 184, 1924.

[2]Jones, R. T., "Properties of Low-Aspect-Ratio Pointed Wings at Speeds Below and Above the Speed of Sound," NACA Rept. 835, 1946.

[3]Ward, G. N., "Supersonic Flow Past Slender Pointed Bodies," *Quarterly Journal of Mechanics and Applied Mathematics,* Vol. 2, 1949, pp. 75–97.

[4]Spreiter, J. R., "The Aerodynamic Forces on Slender Plane- and Cruciform-Wing and Body Combinations," NACA Rept. 962, 1950.

[5]Barnwell, R. W., "Extension of Hypersonic, High-Incidence, Slender-Body Similarity," *AIAA Journal,* Vol. 25, Nov. 1987, pp. 1519–1522.

[6]Sychev, V. V., "Three-Dimensional Hypersonic Gas Flow Past Slender Bodies at High Angles of Attack," *Journal of Applied Mathematics and Mechanics,* Vol. 24, 1960, pp. 296–306 (English translation).

[7]Heaslet, M. A., and Spreiter, J. R., "Three-Dimensional Transonic Flow Theory Applied to Slender Wings and Bodies," NACA Rept. 1318, 1957.

[8]Ashley, H., and Landahl, M., *Aerodynamics of Wings and Bodies,* Addison-Wesley, Reading, MA, 1965.

[9]Hemsch, M. J., "An Improved, Robust, Axial Line Singularity Method for Bodies of Revolution," AIAA Paper 89-2176, Aug. 1989.

[10]Band, E. G. U., and Payne, P. R., "The Pressure Distribution on the Surface of an Ellipsoid in Inviscid Flow," *Aeronautical Quarterly,* Feb. 1980, pp. 70–84.

[11]Wang, K. C., "Three-Dimensional Boundary Layer Near the Plane of Symmetry of a Spheroid at Incidence," *Journal of Fluid Mechanics,* Vol. 43, 1970, pp. 187–209.